Upstream cyclone influence on the predictability of block onsets over the Euro-Atlantic region

Article

Published Version

It is advisable to refer to the publisher's version if you intend to cite from the work. See Guidance on citing.

CentAUR

Central Archive at the University of Reading

Reading's research outputs online

Upstream Cyclone Influence on the Predictability of Block Onsets over the Euro-Atlantic Region

J. W. Maddison and S. L. Gray

Department of Meteorology, University of Reading, Reading, United Kingdom

O. Martínez-Alvarado

National Centre for Atmospheric Science, and Department of Meteorology, University of Reading, Reading, United Kingdom

K. D. Williams

Met Office, Exeter, United Kingdom

ABSTRACT

Atmospheric blocking has been shown to be a phenomenon that models struggle to predict accurately, particularly the onset of a blocked state following a more zonal flow. This struggle is, in part, due to the lack of a complete dynamical theory for block onset and maintenance. Here, we evaluate the impact cyclone representation had on the forecast of block onset in two case studies from the North Atlantic Waveguide and Downstream Impact Experiment field campaign and the 20 most unpredictable block onsets over the Euro-Atlantic region in medium-range forecasts from the ECMWF. The 6-day forecast of block onset in the case studies is sensitive to changes in the forecast location and intensity of upstream cyclones (one cyclone for one case and two for the other case) in the days preceding the onset. Ensemble sensitivity analysis reveals that this is often the case in unpredictable block onset cases: a one standard deviation change in 1000-hPa geopotential height near an upstream cyclone, or 320-K potential vorticity near the tropopause, two or three days prior to block onset is associated with more than a 10% change in block area on the analyzed onset day in 17 of the 20 onset cases. These results imply that improvement in the forecasts of upstream cyclone location and intensity may help improve block onset forecasts.

1. Introduction

Atmospheric blocking events are associated with extended periods of anomalous weather (e.g., Rex 1951; Trigo et al. 2004) and can influence weather in regions downstream (e.g., Carrera et al. 2004; Galarneau et al. 2012). Blocking events can also have severe societal impacts (Kirsch et al. 2012) so forecasting the onset of a blocked period at the longest lead time possible is of large socioeconomic interest and has been the focus of much research. However, a complete dynamical theory

of blocking does not yet exist (Woollings et al. 2018) so forecasting accurately is a well-documented challenge (e.g., Pelly and Hoskins 2003). Ferranti et al. (2015) showed that among large-scale weather regime transitions, the transition to a blocked state following a more zonal flow was the most difficult to predict. The forecast of the frequency of blocking during winter has shown to be underrepresented in several numerical weather prediction (NWP) models and for many years (Tibaldi and Molteni 1990; Matsueda 2009). Increasing model resolution (e.g., Matsueda et al. 2009; Anstey et al. 2013; Schiemann et al. 2017), improving the parameterization of subgrid physical processes (e.g., Palmer et al. 1986;

ⓐ Denotes content that is immediately available upon publication as open access.

Corresponding author: J. W. Maddison, j.maddison@pgr.reading.ac.uk

Jung et al. 2010; Dawson and Palmer 2015; Pithan et al. 2016), and removing model biases (e.g., Kaas and Branstator 1993; Scaife et al. 2010; Zappa et al. 2014) have been shown to improve the representation of blocking in modeling systems, although current models still exhibit errors (Davini and D'Andrea 2016). The representation of atmospheric blocking has also been shown to be closely related to the representation of upper-level Rossby waves (e.g., Austin 1980; Altenhoff et al. 2008; Martínez-Alvarado et al. 2018), which have been shown to be systematically misrepresented in several NWP models (Gray et al. 2014). In this study, we explore the relationship between errors in forecasts of block onset over the Euro-Atlantic region and upstream flow features, with a focus on upstream cyclones.

Upstream cyclones are important in the development and maintenance of atmospheric blocking. The thermal and vorticity advection associated with these systems forces geopotential height rises and the anticyclonic growth of incipient blocks (Colucci 1985; Nakamura and Wallace 1993). Their continual transfer of momentum and vorticity forcing can act to maintain blocks against dissipation (Shutts 1983). The phase of synoptic-scale cyclones relative to planetary-scale waves can determine whether a block onset occurs (e.g., Colucci 1987), with an upstream shift of one-quarter wavelength from the block being favorable (Austin 1980; Mullen 1987). Baroclinic instability in the storm-track regions is primarily responsible for producing the synoptic-scale cyclones (Mullen 1987). Additionally, the vast majority of blocking anticyclones are preceded by a cyclone (Colucci and Alberta 1996). For example, Lupo and Smith (1995) found that *all* of the 63 blocking events in their climatology of Northern Hemisphere wintertime blocking anticyclones could be identified as having an upstream precursor cyclone. Michel et al. (2012) found that, during the onset of Scandinavian blocking, cyclones move in a straight line northeastward across the Atlantic and have high intensity near Greenland. The background flow during Scandinavian blocking onset is strong enough to prevent the cyclonic wrap-up of potential vorticity (PV) around the cyclones, which results in anticyclonic Rossby wave breaking over Europe. Due to the fact that not every intense synoptic-scale cyclone is accompanied by the onset or maintenance of a block, and the highly idealized nature of earlier studies (e.g., Shutts 1983), Yamazaki and Itoh (2009) proposed a new selective absorption mechanism for block maintenance, whereby blocking highs selectively absorb anticyclonic synoptic-scale eddies, as they are of the same polarity as the blocks, reinforcing their own PV as a result. The selective absorption mechanism is seen as useful because it can be adapted for both dipole- and Ω-type

blocks and shifts in the storm-track location, and it has been verified for observed cases of blocking (Yamazaki and Itoh 2013). The onset of blocking can also be triggered by planetary-scale waves. Forcing from a quasi-stationary Rossby wave train can be the dominant driver of block onset over Europe (Nakamura et al. 1997), with these wave trains frequently emanating from the subtropical western Atlantic (Michel and Rivière 2011). Interactions between the planetary and synoptic scales were shown to play a substantial role in block formation in an observational case study by Tsou and Smith (1990) and whether a block onset occurs can depend on the phase of background planetary waves relative to the synoptic-scale surface cyclone and their amplitude (Colucci 1987).

Cyclones have also been studied for their role in the amplification of tropospheric ridges and how their associated moist processes are key for tropopause-level development and realizing highly amplified flow. Diabatic processes embedded in cyclones modify the PV structure in the warm conveyor belt (WCB) (Joos and Wernli 2012) and around the tropopause (Davis et al. 1993; Ahmadi-Givi et al. 2004; Chagnon et al. 2013), with a negative tendency above the region of maximum heating acting to enhance downstream ridges (Tamarin and Kaspi 2016). Modifying the PV structure near the tropopause alters Rossby wave propagation (Harvey et al. 2016). Diabatic processes also amplify upper-level ridge-building events downstream of recurving ex–tropical cyclones in the North Atlantic (Grams et al. 2011) and Pacific (Grams and Archambault 2016). The observed highly amplified flow that can occur in these cases can only be realized as a result of the cross-isentropic ascent of air mass associated with latent heating in the WCBs of the ex–tropical cyclones. The representation of diabatic processes in an NWP model was also shown to be responsible for the forecast underamplification of a large-amplitude ridge by Martínez-Alvarado et al. (2016). Furthermore, air ascending cross isentropically was shown to contribute considerably to blocked air masses by Pfahl et al. (2015), who found that more than 50% of air masses that formed blocking events in the ECMWF interim reanalysis (ERA-Interim, hereafter ERA-I) (Dee et al. 2011) had undergone considerable ascent and diabatic heating in the days prior to arrival in the block. Air ascending into blocking anticyclones at high latitudes in the WCBs of recurrent extratropical cyclones can also be important in driving extreme events (Binder et al. 2017).

While the mechanistic link between upstream cyclones and blocking has been studied, less attention has been paid to their relationship in terms of predictability, or how upstream cyclones affect forecasts of blocking.

A few case studies have been analyzed, but little systematic analysis has been performed. For example, Grams et al. (2018) showed for a block forecast over Europe in the ECMWF Ensemble Prediction System (EPS), that error in the intensity of the WCB in a cyclone simulated by the ensemble, which was shown to be related to an error in the structure of an upper-level trough, resulted in the poor forecast of the upper-level Rossby wave structure over Europe. For a case study over the Rockies, Matsueda et al. (2011) showed that the forecast of a cutoff cyclone upstream of the block was essential for the accurate development of blocking. The forecast of the block was shown to be sensitive to perturbations in the region of the cutoff cyclone and modifying the perturbations were shown to improve the block development. Forecasting blocking is important because blocks have been shown to be the cause of some of the poorest forecasts, so-called *forecast busts*, for Europe during recent years: occasions when forecasts from one (or several) NWP centers experience a period of unusually low forecast skill. Rodwell et al. (2013) looked at forecast busts occurring over Europe in a 22-yr period from forecasts from ERA-I. Their composite 500-hPa geopotential height (Z500; equivalent notation also used for geopotential height at other pressure levels) field for all the bust cases resembles a block over Europe. Forecast bust cases were shown to be associated with a trough over the Rocky Mountains and increased convective available potential energy (CAPE) over North America released within mesoscale convective systems (MCSs) in that region, at initialization time six days earlier. Blocking was also shown to be a large contributor to forecast bust cases by Lillo and Parsons (2017). Using the same set of bust cases as Rodwell et al. (2013), they clustered the bust cases into four subsets based on their 6-day forecast evolution over the North Atlantic using a clustering algorithm. At the time of forecast initiation, two of the clusters resembled blocking patterns over the United States and Europe and, at the time of verification, the other two clusters resembled blocking features. This implies that transitions to and from a blocked situation are times when the model can have large uncertainties and large forecast errors, consistent with the study by Ferranti et al. (2015). Both Rodwell et al. (2013) and Lillo and Parsons (2017) go further and suggest a relationship between large forecast errors over Europe and upstream Rossby wave activity forcing. In summer this is typically associated with MCSs, in autumn with recurring tropical cyclones, and in winter with extratropical cyclogenesis. The convection active in each of these cases is not well represented in the ECMWF model and its influence on the downstream

propagation of Rossby waves (via PV modification at upper levels) can result in large forecast errors.

The relationship between a specific forecast feature of interest and earlier atmospheric features can be quantified using ensemble sensitivity or adjoint sensitivity methods. The fundamental goal in both methods is to determine where small perturbations in a precursor field can result in large changes in a response function later in the forecast. For example, Yang et al. (1997) used adjoint sensitivity analysis to show blocking over central and eastern Russia was sensitive to upstream perturbations in the streamfunction field. Sensitivity methods have also been used, for example, to determine sources of initial condition error (Torn and Hakim 2008), target useful observation locations (Ancell and Hakim 2007), identify climatological characteristics associated with cyclone development (Dacre and Gray 2013), and identify the origin of forecast errors in forecast bust cases over Europe (Magnusson 2017). Magnusson (2017) looked at three particular forecast bust cases in the ECMWF EPS and identified regions in the Z200 or Z500 fields in which these errors originated. The final case in Magnusson (2017) was a forecast bust resulting from an underestimated blocking ridge over Scandinavia. The error origin was found to be over the western Atlantic, where extratropical cyclone activity is frequent. The error in the block forecast in this case was attributed to error in the WCB representation by Grams et al. (2018). Error growth and forecast sensitivity can also be studied using tangent linear methods. Frederiksen (1998) found that a case of blocking over the North Atlantic was associated with the enhanced development of perturbations located upstream off the east coast of North America, a region where cyclogenesis has been observed to trigger block onset (Colucci 1985). Cyclogenesis off the east coast of North America was also suggested to trigger the large-scale, baroclinic instability modes of a multilevel quasigeostrophic model that were associated with the onset of blocking by Frederiksen and Bell (1990).

The two case studies explored in detail here are related to the North Atlantic Waveguide and Downstream Impact Experiment (NAWDEX; Schäfler et al. 2018). This recent international field campaign investigated the role of diabatic processes in modifying the upper-level Rossby wave pattern and the jet stream and influencing high-impact weather downstream. Four research aircraft and a host of ground-based instruments were utilized to observe these processes to improve our understanding of Rossby wave dynamics and the role of diabatic processes. During the campaign period, 17 September–22 October 2016, a wealth of weather phenomena were observed, including tropical cyclone

transition into the extratropics, tropopause polar vortices, atmospheric rivers, and a large, very persistent atmospheric block. This block, one of the case studies here, was an important feature in NAWDEX as it persisted over Scandinavia for much of the campaign.

The aim of this study is to systematically investigate the link between forecasts of block onset and upstream flow features with a focus on the influence of upstream cyclone activity on the forecast of block onset. The question is whether the location and intensity of an upstream cyclone in the days preceding block onset are important for the block appearing in the forecast. In section 2, we give details of the forecast data used in this study and describe the blocking index, ensemble sensitivity technique, and trajectory calculation. Section 3 contains an analysis of the NAWDEX block case study. In section 4, a second case study is briefly presented to highlight some case-dependent differences between block onset forecasts and upstream cyclone activity. We extend the analysis to 20 of the most uncertain block onsets occurring in the autumns and winters from 2006 to 2017 in section 5. In section 6, we summarize the findings of this analysis and discuss some of their implications.

2. Data and methods

a. Operational forecast data

The THORPEX Interactive Grand Global Ensemble (TIGGE; Bougeault et al. 2010) is an archive containing operational ensemble forecast data from 10 NWP centers dating from 2006 to the present that is updated quasi operationally. Daily 0000 and 1200 UTC forecasts of Z1000, Z500, and potential vorticity on the 320-K isentropic surface (PV320) during autumn and winters (from 1 September 2006 to 28 February 2017) from the ECMWF EPS (Molteni et al. 1996; Buizza et al. 1999) accessed via the TIGGE archive are used in this study. Potential vorticity is only available at 320 K in TIGGE. However, Madonna et al. (2014) showed that cross-isentropic ascent in WCBs can reach at least 315 K in winter (with mean values between 313 and 321 K) so using PV320 to consider WCB outflow in autumn and winter is reasonable, though not optimal for early September cases where WCB outflow may reach higher levels. Block onsets occurring only in autumn and winter were chosen for this study as extratropical cyclones are more frequent and intense over the Euro-Atlantic region during these seasons. ERA-I data are used for verification of the ECMWF EPS forecasts. All forecast and reanalysis data are interpolated onto a common 1° grid. Six-hourly ECMWF operational analysis data (winds, surface pressure, and specific humidity) are used in the trajectory calculations (section 2d).

b. Block onset identification

1) BLOCKING INDEX

The 2D Z500 blocking index introduced by Scherrer et al. (2006), based on the 1D index by Tibaldi and Molteni (1990), is used in this study. The index is calculated using the northern and southern gradients in Z500, termed northern geopotential height gradients (GHGN) and southern geopotential height gradients (GHGS). The gradients are calculated at each longitude for latitudes (ϕ_0) between 35° and 75°N:

$$\text{GHGN} = \frac{Z(\phi_N) - Z(\phi_0)}{\phi_N - \phi_0} \quad \text{and}$$
$$\text{GHGS} = \frac{Z(\phi_0) - Z(\phi_S)}{\phi_0 - \phi_S},$$

where $\phi_S = \phi_0 - 15°$ and $\phi_N = \phi_0 + 15°$. A latitude–longitude grid point is then defined as being blocked if GHGS > 0 and GHGN < −10 (m per degree). A schematic showing an example Z500 field that satisfies these criteria is shown in Fig. 1 of Martínez-Alvarado et al. (2018).

In this study, the blocking index is used to identify the date of block onset in the Euro-Atlantic region (defined as 40°–75°N, −60°–50°E). This region is chosen to be large with the aim of identifying only true block onsets, rather than blocked areas that move in or out of the domain (though this still can occur). The Euro-Atlantic region is defined as blocked at a given time if the largest area identified as blocked by the index exceeds an arbitrary value. The threshold is chosen to represent the typical area that the index identifies as blocks within large-scale blocking ridges in the tropopause. Considering several cases of blocking events, the threshold chosen is 950 000 km^2 (approximately the area of a circle of 10° at 60°N), though the choice of this threshold is subjective as there is no universally accepted area that defines a block. Woollings et al. (2018) used 500 000 km^2 to define the area of a block while earlier studies have defined the scale of a block based on its longitudinal span, ranging from 12° (Tibaldi and Molteni 1990) to 45° (Rex 1950). The date of a block onset is then defined as the first day of a period of at least four days identified as blocked in the Euro-Atlantic region that follows four days of the region being not blocked. This criterion gives 34 blocking events during the study period (defined in section 2a).

2) UNCERTAIN BLOCK ONSETS

Block onsets that had large uncertainty in their 6-day forecast were chosen for analysis in this study. Uncertainty was measured using the area identified as blocked

by the index in 6-day ensemble forecasts from the ECMWF EPS for the date of block onset in ERA-I. The 25 most uncertain onsets, defined as those with the largest interquartile range of block area in the ensemble, were chosen for analysis in this study. We focus on the most uncertain cases because a large range of block areas within the ensemble improves the reliability of the ensemble sensitivity analysis. However, five of the onsets were discarded: three for being blocking events moving in and out of the North Atlantic–European domain and hence not considered real block onsets and two because the index identified features that a synoptician would not call a block. In one of the false cases the index was triggered over Greenland to the north of a large-scale trough with no ridge feature in that region. The other false case was caused by a large trough over Scandinavia to the west of a ridge that extended outside of the domain.

c. Ensemble sensitivity

1) CALCULATION

The ensemble sensitivity method used here follows the approach of Garcies and Homar (2009). The response function J is chosen here to be the area diagnosed as blocked by the blocking index. It is calculated for each ensemble member (51 members) for forecasts of a chosen lead time, here six days. The sensitivity $S_{i,j}$ is calculated as

$$S_{i,j} = m_{i,j} \times \sigma_{i,j} \times \alpha_{i,j} = \frac{\text{cov}(x_{i,j}, J)}{\sigma_{i,j}} \times \alpha_{i,j},$$

where

$$m_{i,j} = \left(\frac{\partial J}{\partial x}\right) i, j,$$

and $x_{i,j} = X_{i,j} - \overline{x}_{i,j}$ (the difference between the forecast field X and the mean of the ensemble forecast $\overline{x}$ at grid point i, j), $\sigma_{i,j}$ is the standard deviation of the precursor field in the ensemble at each grid point, and $\alpha_{i,j}$ is a correction factor applied to filter out weak correlations (the method assumes linearity) between the response function and the precursor minus mean field:

$$\alpha_{i,j} = \begin{cases} 1, & \text{if } r_{i,j}^2 \geq r_{\min}^2 \\ \dfrac{r_{i,j}^2}{r_{\min}^2}, & \text{if } r_{i,j}^2 \leq r_{\min}^2 \end{cases},$$

where $r_{i,j}$ is the correlation coefficient and $r_{\min}^2$ is the minimum correlation coefficient for which the raw sensitivities remain unaltered. Here $r_{\min}^2$ is chosen as 0.15

to only retain reliable sensitivity information and to produce clear sensitivity fields, but the conclusions are robust with $r_{\min}^2 = 0.05$. We have used the property

$$m_{i,j} = \frac{\text{cov}(x_{i,j}, J)}{\text{var}(x)_{i,j}},$$

resulting from the least squares regression calculation in the above (note that $J = J_{i,j} \forall i, j$).

The sensitivity has the same units as the response function, in this case meters squared. The sensitivity value can be interpreted as the change in response function due to a one standard deviation increase in the precursor field. Multiplication by the standard deviation also takes into account the climatologically lower variance at lower latitudes and prevents misleading climatological sensitivity values [see Garcies and Homar (2009) for more details]. For this study, the sensitivity values detail how the area of the block in the ensemble (six days into forecast run) changes as a result of a one standard deviation change in a given precursor field (three–four days into forecast run).

Magnusson (2017) used a similar ensemble sensitivity calculation in their evaluation of three forecast bust cases over Europe. They calculated the sensitivity as the correlation between the response function and precursor field,

$$S_{i,j} = \frac{\text{cov}(J, x_{i,j})}{\sigma_{i,j} \sigma_J},$$

which differs from our calculation by a factor of $\sigma_J \alpha_{i,j}$, where σ_J is the standard deviation of the response function in the ensemble. The $\alpha_{i,j}$ term is simply a damping term so the patterns (and signs) of the sensitivity fields will not change on its application, but sensitivity values in regions where the correlation between the response function and precursor field is weak will be reduced in magnitude. The σ_J term takes into account the size and spread of the response function in the ensemble. Here, we present the sensitivities as percentage departures from the response function value in ERA-I, so information about the response function is included in our calculation and the resulting sensitivities are very comparable with the method used in Magnusson (2017).

2) CHOICE OF RESPONSE FUNCTION

Ensemble sensitivity analysis results are presented here using the area blocked in the blocking index as the response function as this provides easily interpretable information about changes in block area due to earlier changes in the forecast evolution. Ensemble sensitivity

is also briefly discussed for two other response functions for comparison and to determine the robustness of the results. The first additional response function used is the root-mean-square error (RMSE) of Z500 over the blocked region. The blocked region is defined as the region between 40° and 80°N and between 30°W–30°E, 0°–60°E, and 60°W–0° for blocks over the United Kingdom, Scandinavia, and Greenland, respectively. Using RMSE of Z500 as the response function gives sensitivity values that detail where earlier changes in a given forecast field are associated with increased or decreased forecast error. The second additional response function used is a measure of ridge area. Ridges are defined as regions north of 55°N, in the same longitudinal bands defined above, where PV320 is less than 2 PVU ($1 \, \mathrm{PVU} = 10^{-6} \, \mathrm{m^2 \, s^{-1} \, K \, kg^{-1}}$). The ridge area response function is used to investigate the relationship between the Z500-based blocking index and ridges in PV320. While the RMSE of Z500 and ridge area response functions provide useful information about forecast sensitivity, they will be affected by processes separate from block dynamics because other features, for example, cyclonic regions upstream or downstream of the blocking high pressure, may dominate their values. This means that the sensitivity cannot be interpreted in terms of blocking directly.

3) INTERPRETATION OF ENSEMBLE SENSITIVITY

In this study ensemble sensitivity analysis is used to determine how the representation of upstream cyclones affect downstream block forecasts. For each block onset forecast, each ensemble member will forecast a different location and intensity of the upstream cyclone (if present). Here, simple idealized sensitivities for a small ensemble are calculated to determine the sensitivity patterns we expect when it is the forecast of the cyclone's strength and/or location that is most important for the downstream block forecast. In each case the ensemble consists of three members, each with a prescribed cyclone location and intensity (minimum Z1000) as well as a value for the response function J (block area). Cyclones are constructed using an idealized Z1000 field modeled as a 2D Gaussian distribution with values of Z1000 > −0.5 m set to zero. The prescribed differences in cyclone location, cyclone intensity, and response function value were chosen based on those seen in the ECMWF EPS forecasts.

Four simple idealizations of cyclone forecast, response function, and sensitivity field are presented in Fig. 1. In the first three examples the response function is chosen so that the cyclone located farthest to the west has the largest block develop downstream and the cyclone farthest to the east has the smallest; in the last

example the ensemble members all have same location and the ensemble member with the deepest cyclone has the largest forecast block.

In the first example only the cyclone location changes among the ensemble (the three cyclones all have the same intensity). In this example the sensitivity pattern is a dipole centered on the middle of the three cyclones. The dipole is symmetric along the axis of cyclone location change with a negative/positive orientation. The negative sensitivity to the west implies increasing Z1000 in this region is associated with a smaller block. This is equivalent (by linearity) to a deeper cyclone in this location being associated with a larger block, as we expected by construction.

In the second example, the cyclone intensity and location are both changed among the ensemble. The western cyclone is made deeper, the central cyclone remains the same, and the eastern cyclone (associated with the smallest block) is weakened. The same negative/positive dipole in sensitivity as for example 1 remains. However, the region of negative sensitivity expands and increases slightly in magnitude while the region of positive sensitivity is reduced.

In the third example, the cyclone farthest east is the strongest cyclone among the ensemble, still with the smallest block. The negative/positive dipole remains, but the positive region of sensitivity is larger and stronger and the negative region of sensitivity is reduced compared to examples 1 and 2. If we had constructed the ensembles in the above examples such that it was the cyclone farthest east that resulted in a larger block, the dipoles would be identical, but with orientation positive/negative, that is, rotated by 180° (not shown).

Finally, in the fourth example we construct an ensemble in which the location of the cyclone is the same in each ensemble member, but the intensity changes. The resultant sensitivity field is a monopole of negative sensitivity around the location of the cyclones. Had we chosen the response function such that the ensemble member with the weakest (rather than the strongest) cyclone had the largest block then the monopole would be positive.

Together, the idealized scenarios presented suggest that changes in response function resulting from differences in cyclone location in the ensemble forecast leads to the sensitivity field to have a dipole structure. Any asymmetries in the dipole are associated with sensitivity to cyclone intensity. If the negative lobe of the sensitivity pattern dominates in the dipole, the deeper cyclones in the ensemble are associated with larger blocks developing downstream; if it is the positive lobe that dominates, then it is the weaker cyclones. This relationship does not depend on the dipole
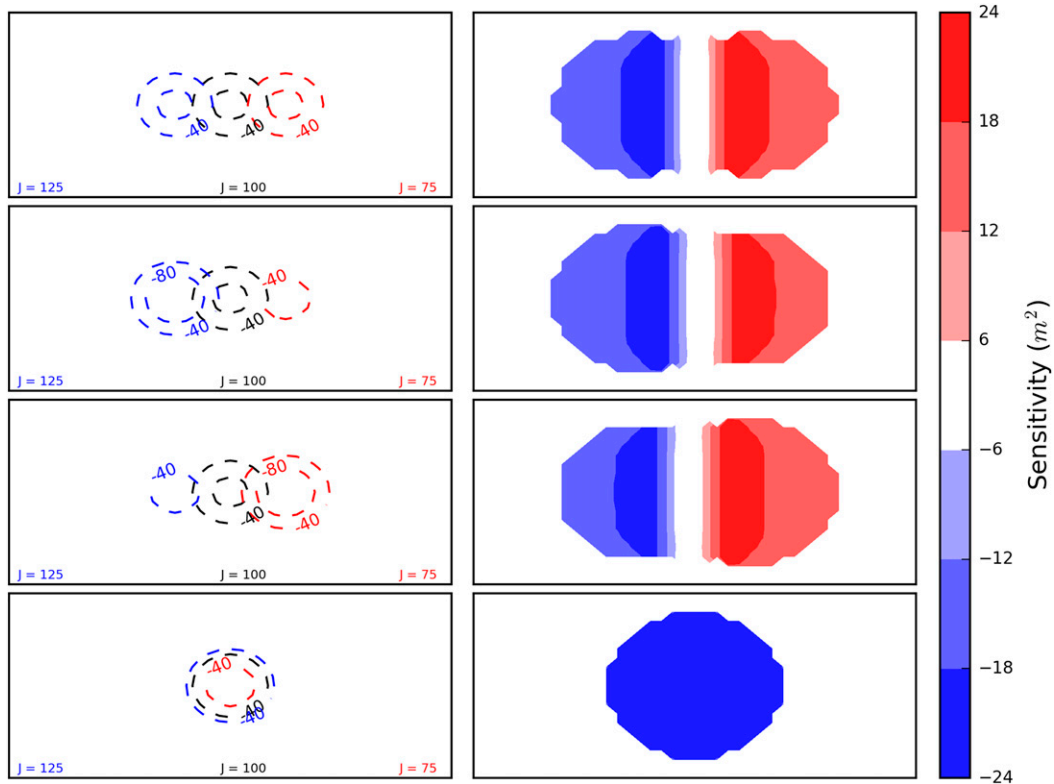
FIG. 1. (left) Four idealized three-member ensemble forecasts of a cyclone and response function *J*, and (right) the corresponding sensitivity field for each ensemble forecast. Contour values of -40 and -80 m Z1000 are presented to identify the cyclones in each ensemble member.

orientation. These results also suggest that a monopole in the sensitivity pattern is associated with larger importance of the intensity of the cyclone in the ensemble forecast rather than its location. The idealized sensitivity fields presented here aid in the interpretation of the results presented in the remainder of this article.

d. Trajectory calculation

Air that has ascended into the blocking ridges in each case is traced backward to an upstream cyclone using trajectories calculated with the Lagrangian Analysis Tool (LAGRANTO; Wernli and Davies 1997; Sprenger and Wernli 2015). Back trajectories are started within the blocking ridge (in the region where the blocking index is satisfied) every 25 hPa from 400 to 200 hPa at 1200 UTC on the date of block onset in ERA-I. The trajectories are calculated backward using the ECMWF operational analysis wind fields for 84 h. Those that descend more than 500 hPa in the first 72 h are classed as part of the WCB and used to identify the cyclone(s) associated with ridge building and block onset. Previous studies (e.g., Grams and Archambault 2016) have used 600 hPa ascent in 48 h to define a WCB.

This criterion is slightly modified here to take into account the fact that we do not a priori know when strong ascent occurred in each case relative to the date of block onset in ERA-I. The cyclone identified is termed here the block's *feeder cyclone*, as it is feeding the blocked air mass. In the case that the back trajectories identify multiple cyclones feeding the blocking ridge then the cyclone with the larger number of trajectories entering the block is chosen. This identification provides a dynamical link between the upstream cyclone and the block and allows us to focus the ensemble sensitivity analysis in the region of the upstream feeder cyclone.

3. Case study I: NAWDEX

The first case study of a block onset that was associated with large uncertainty occurred on 4 October 2016 during the NAWDEX field campaign. In this section, a description of the synoptic evolution in the days preceding block onset is given together with an analysis of the operational ensemble forecast performance of the ECMWF EPS in the days leading to the onset of the block. An illustration of the role an
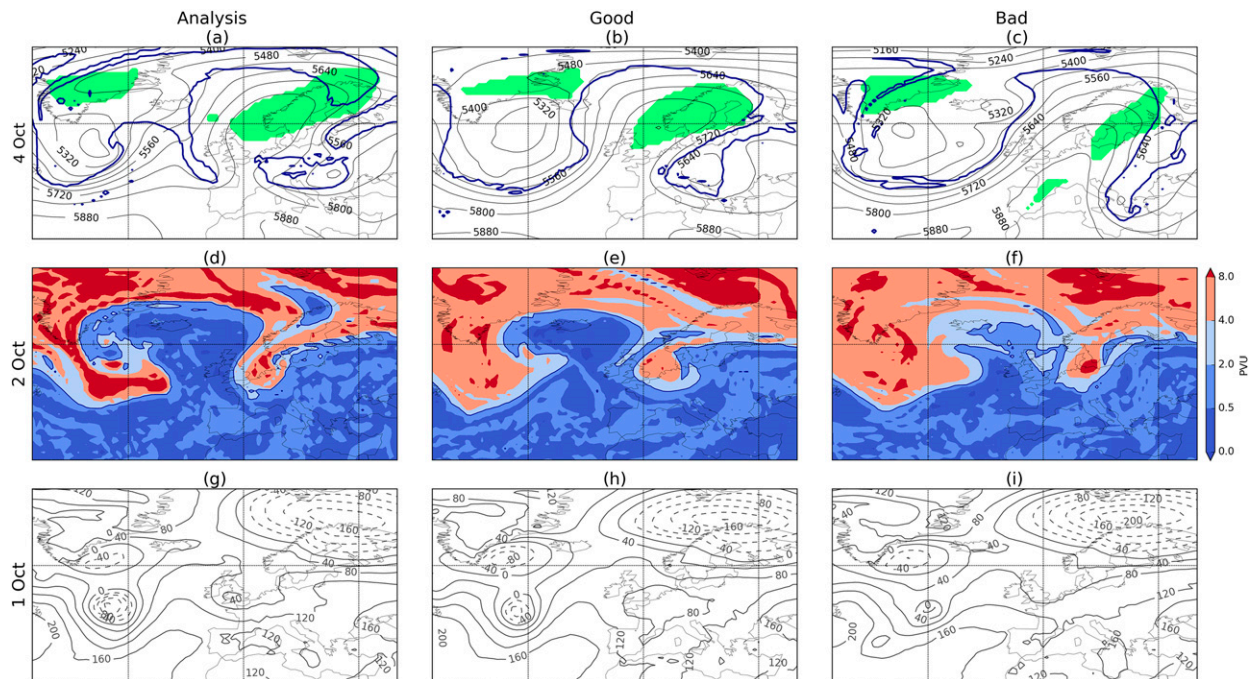
FIG. 2. (a)–(c) Z500, the 2-PVU contour, and blocking index (green shading) on 4 Oct 2016, (d)–(f) PV320 on 2 Oct 2016 showing tropospheric (blues) and stratospheric (reds) air, and (g)–(i) Z1000 on 1 Oct from (left) ERA-I and (middle),(right) in the forecast initiated on 28 Sep 2016 from two members of the ECMWF EPS.

upstream cyclone had on the forecast evolution in the days leading to block onset is presented together with ensemble sensitivity analysis results for the block onset to conclude this section.

a. Overview of synoptic situation

The days preceding the block onset were a period of intense weather activity over the Euro-Atlantic region. A block had been situated over Scandinavia since the beginning of September and broke down around 25 September. A deep cyclone, named the Stalactite cyclone during the NAWDEX campaign because of the very deep, narrow, stalactite-like tropopause trough associated with it, was located over the North Atlantic Ocean (to be discussed in section 3b) on 1 October and was moving toward Iceland (Fig. 2g). The system had a strong WCB (to be discussed in section 3b) that amplified the upper-level ridge ahead of it and on 2 October 2016 there was a large-amplitude ridge in the tropopause extending across a large part of the North Atlantic (Fig. 2d). This ridge became the blocking ridge that formed over Scandinavia on 4 October (Fig. 2a). The block persisted over Scandinavia for several weeks. The development of the Stalactite cyclone and the subsequent onset of blocking was identified as a highlight of the NAWDEX field campaign in Schäfler et al. (2018) (see their sequence B for more details) and

the Stalactite cyclone and its WCB were observed by the campaign aircraft during several phases of their development.

b. Forecast representation

The onset of the NAWDEX block was associated with large forecast uncertainty: forecasts valid for the time of block onset experienced an extended reduction in anomaly correlation coefficient of Z500 over Europe (Schäfler et al. 2018). The 6-day forecast of the area identified as blocked over Europe had large spread among the ensemble. The size of the largest area identified as blocked in each ensemble member of the ECMWF EPS as the forecast evolves is presented in Fig. 3. The area in each ensemble member and the control forecast is calculated in the region of the block in the analysis (40°–50°N, 10°W–40°E). The majority of the ensemble members underpredicted the area of the block that formed compared to ERA-I, or did not predict a block onset at all. The control member matches the evolution seen in ERA-I reasonably well, apart from the underestimation of the size of block on the onset date and a delay in the increase in block area that occurs after 96 h in ERA-I. The ensemble members show large spread: some members have a large area blocked early into the forecast run and nearly all underpredict the block area on block onset date.
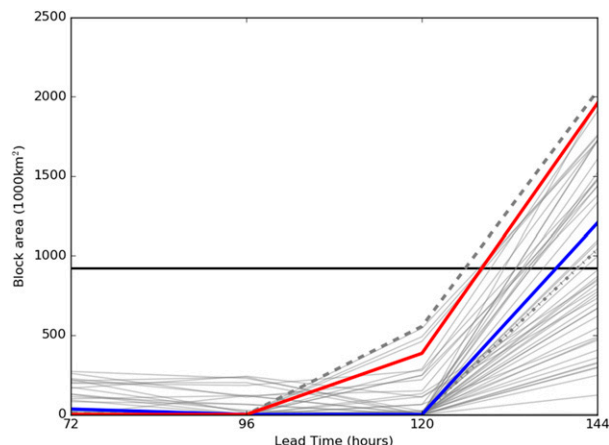
FIG. 3. Area of the largest object identified as a block between 72- and 144-h lead time in the forecast initiated on 28 Sep 2016 from the ECMWF EPS for the NAWDEX case study. The area is shown for each ensemble member (gray lines), the control member (blue line), and in ERA-I on the corresponding date (red line). The good and bad ensemble member (see text) are shown with the dashed and dash–dotted lines respectively.

We hypothesize that this misrepresentation was caused by the earlier poor forecast of the upstream Stalactite cyclone. To demonstrate that this may be the case it is helpful to consider the flow evolution in two ensemble members from this ECMWF EPS forecast and compare their development to that seen in ERA-I. The two ensemble members were chosen as having either similar or different block representation to ERA-I six days into their forecast (based on RMSE of Z500 averaged over Europe, 62 and 139 m for the chosen members, and similarity of block area to ERA-I): these are named the good and bad ensemble members, respectively, though both represent possible evolutions of the system. The area identified as blocked in the good and bad ensemble members is highlighted in Fig. 3. In Fig. 2, Z1000 on 1 October 2016, PV320 on 2 October 2016 and Z500, the tropopause at 320 K (taken as the 2-PVU surface) and blocking index on 4 October 2016 are shown for the analysis and forecasts of the corresponding date from the good and bad ensemble members. The block is clearly identifiable in the analysis as a large-scale tropospheric ridge in both the tropopause contour and Z500 field (Fig. 2a). The index identifies the block of interest over a large region from the north of the United Kingdom to Scandinavia as well as a second center of blocking action over Greenland. The blocking ridge in PV320 is also present in both ensemble members but is less amplified, particularly in the bad ensemble member in which the ridge extends less far to the north and spans fewer longitudes. Two days prior to block onset the underamplification of the ridge in the

forecasts is more obvious. The ridge in the analysis extends much farther poleward than in either of the ensemble members and a PV streamer has formed on the western flank of the ridge which is not present in either ensemble member. The good ensemble member has a larger, more coherent ridge than the bad ensemble member, but it is still not as amplified as in the analysis and in the bad member this results in a delay in the block onset (Fig. 3).

The smaller ridges in the ensemble member forecasts are consistent with the underestimation of the Stalactite cyclone intensity and incorrect location of the cyclone relative to the upper-level features. In the analysis the cyclone was much deeper and located farther west than in either of the ensemble members. We hypothesize that this affected the development of the upper-level ridge. A stronger system could amplify the ridge more due to a number of mechanisms. A stronger WCB with stronger latent heating will lead to inflow air arriving at higher altitudes and having a larger negative PV anomaly relative to the background PV. Because the average PV of the outflow of a WCB almost equals that of the inflow (Methven 2015), it will be associated with stronger upper-level divergence. A stronger system will also have greater advection of low-valued PV air from the south to the north. The WCB of the Stalactite cyclone as represented in the ECMWF analysis is shown in Fig. 4. The Stalactite cyclone's WCB transported a large air mass poleward and upward into the blocking ridge. It is hypothesized that the different WCBs in the ensemble member forecasts are responsible for the different ridge developments. The good ensemble member had a deeper cyclone located farther to the west than the bad member, though not as far west as in the analysis, which is consistent with its more amplified ridge on 2 October. Therefore the forecast of the Stalactite cyclone on 1 October 2016 is likely to have been important for the forecast of the block onset on 4 October 2016. To quantify the extent to which upstream cyclone representation is modifying block representation, ensemble sensitivity analysis is calculated for this onset case.

c. Ensemble sensitivity

We calculate sensitivity to Z1000 and PV320 in the days prior to block onset as these fields can describe upstream flow features, cyclone characteristics, and upper-level development.

The sensitivity of block area at 144 h into the forecast evolution to the earlier forecast of Z1000 is shown in Fig. 5. Sensitivity fields at 72 and 96 h into the forecast evolution are presented with the control forecast overlain to identify features of interest. The region of highest
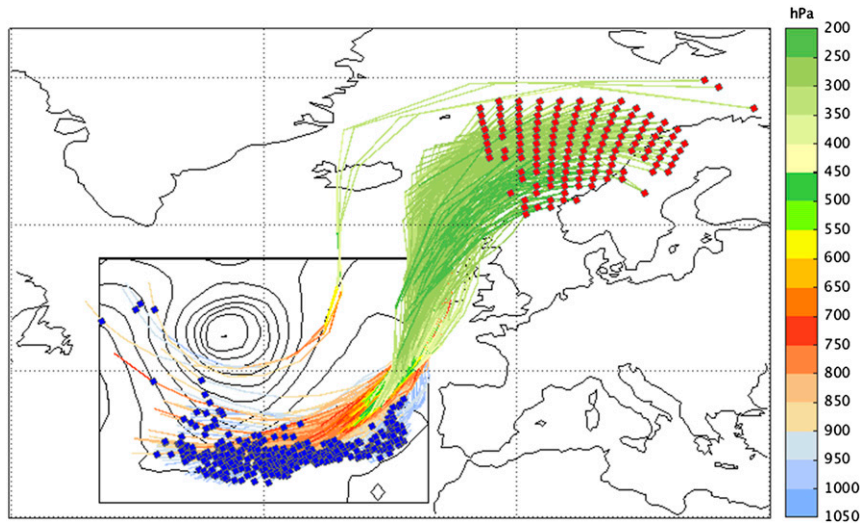
FIG. 4. Backward trajectories initialized within the block (red points) at 1200 UTC 4 Oct 2016 and calculated for 84 h. Trajectory locations are shown for the start points (red points) and at −72 h (blue points). The surface pressure in the region of the cyclone at the time of the blue points is shown by the contours in the region around the cyclone (black box).

sensitivity is located upstream of block location in a dipole around the Stalactite cyclone in the Atlantic, with a region of positive sensitivity to the east of the cyclone center and negative sensitivity to the west of the cyclone in the control forecast. A one standard deviation change in Z1000 is associated with a 15%–20% change in block area forecast relative to the block area in ERA-I. The maximum sensitivity region moves with the cyclone as the forecast evolves (Fig. 5). Recall that positive/negative sensitivity values do not mean that the forecast was

better or worse, but instead that there was more or less blocking in the ensemble members.

The dipole structure of sensitivity in the region of the cyclone can be understood by comparison to the idealized results in section 2c(3). The positive region to the east of the center of the Stalactite cyclone in the control forecast indicates that higher pressure there results in more blocking. The idealized examples show that this is achieved when the cyclones in the ensemble members leading to the largest blocks are located farther west.
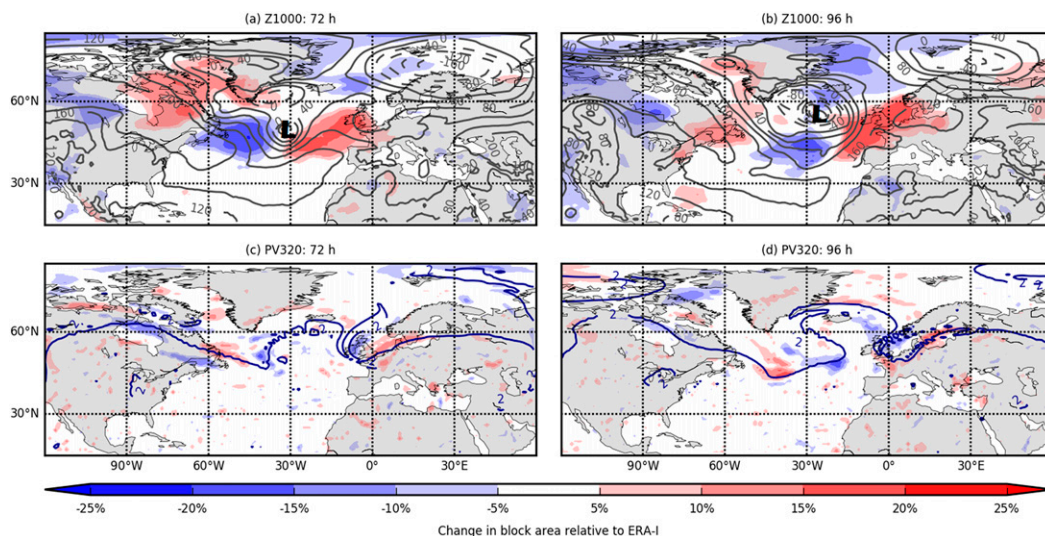

FIG. 5. Sensitivity of the response function 144 h into the forecast initiated at 1200 UTC 28 Sep 2016 to Z1000 at (a) 72- and (b) 96-h lead time and PV320 at (c) 72- and (d) 96-h lead time. The control member forecast of (a),(b) Z1000 or (c),(d) the 2-PVU contour is overlain.

The sizes and strengths of the poles are dependent on lead time. At 72-h lead time the negative pole of the dipole is stronger than the positive pole (Fig. 5a) which implies the ensemble members with the cyclones farther west and more intense have larger blocks than those farther east and less intense. The conclusion that ensemble members that had more intense cyclones located farther to the west (than the cyclone in the control forecast) had a larger blocked area on onset day is consistent with our initial two-member analysis (comparing the good and bad ensemble members for which the good member had the largest block and was closest to the analysis). These results suggest that changes to the location and intensity of the Stalactite cyclone among the ensemble are important for block forecast downstream and we hypothesize that it is changes to the cyclone's WCB structure that lead to the different block structures. Consistent with this hypothesized link between cyclone and WCB intensity, Binder et al. (2016) found a moderate to strong correlation between cyclone intensification and WCB strength.

The sensitivities to PV320 for the same lead times are also shown in Fig. 5. The sensitivity to PV320 is centered on the tropopause and is generally weaker than the sensitivity to Z1000. Sensitivity along the tropopause indicates that the phasing and structure of the upstream Rossby wave pattern is associated with differing representation of the blocking ridge, as we might expect. The increased localized sensitivity around the edge of the blocking ridge and near the upstream trough at both lead times (Figs. 5c,d) implies that the location and extent of the building ridge and upstream trough in the ensemble are associated with changes in the ensemble for block forecast. A region of negative sensitivity on the western flank of the ridge is present at both lead times: increased PV in this region results in a smaller block developing. By linearity, this indicates that if the PV in that region is decreased (i.e., that region becomes part of the ridge) then the area blocked will be larger. It is hypothesized that the ridge building in this case is associated with the divergent outflow from the Stalactite cyclone. There is a region of negative PV advection by the divergent wind on the northern and western flank of the ridge in the deterministic forecast at 96 h and at 250 hPa (not shown), suggesting that the sensitivity in this region could be associated with the representation of the cyclone in the ensemble. The other main region of sensitivity is positive and is present in the location of a shortwave trough (located near 40°N, 40°W at 96 h) upstream of the blocking ridge. Consistent with this sensitivity, the increased cyclonic circulation from a stronger trough would steer the Stalactite cyclone farther to the north and allow for a larger ridge to build.

In summary, for the NAWDEX block onset ensemble sensitivity analysis reveals that an upstream cyclone is clearly identifiable as the main feature influencing the block forecast. Consistent conclusions can be made looking at sensitivity to Z1000 and PV320.

4. Case study II: NAWDEX dry run

The second case study of block onset, referred to here as the NAWDEX dry run block, occurred a year prior to the NAWDEX campaign, during a campaign forecast and flight planning test period. It is included briefly here to demonstrate a more complicated link between block onset and upstream cyclone activity than found for the first case study. The NAWDEX dry run block formed on 27 September 2015, downstream of a merging of a cyclone propagating across the North Atlantic and another near Greenland (the two merging cyclones are visible in the control forecast of Z1000 in Figs. 6a and 6b).

The sensitivity of the block area to Z1000 and PV320 in the days preceding block onset is shown in Fig. 6 for the forecast initiated at 1200 UTC 21 September 2015. At 72 h into the forecast (Fig. 6a), the regions of highest sensitivity extend farther upstream than in the first case study and the highest values are located over North America and between Greenland and Iceland. There is increased localized sensitivity in a dipole around a cyclone propagating across the Atlantic that had a WCB feeding into the block (WCB trajectories not shown). At 96 h into the forecast (Fig. 6b), the high-sensitivity region is now oriented in a dipole with stronger negative sensitivity ahead of the merging cyclones, implying a more intense merging of the two cyclones results in more blocking. The increased sensitivity to Z1000 over North America could be associated with convection in that region: areas of strong convection were present to the west of the Great Lakes and to the northeast of Florida between 24 and 25 September (not shown). The intensity of convection, as inferred from large values of CAPE, was shown to be associated with large forecast errors in Rodwell et al. (2013), though further investigation of the role of this convection is beyond the scope of this study.

The regions of highest sensitivity to PV320 are located in the region near the tropopause: on the western flank of the developing blocking ridge that forms over the United Kingdom and also over North America in similar locations to those of the high sensitivity to Z1000. The sensitivity to PV320 for this case is much stronger than in the NAWDEX case study (cf. Figs. 6c,d with Figs. 5c,d). At 72 h into the forecast (Fig. 6c), the region of large positive sensitivity on the western flank of the blocking ridge over the Atlantic implies that ensemble members with larger magnitude PV320 in
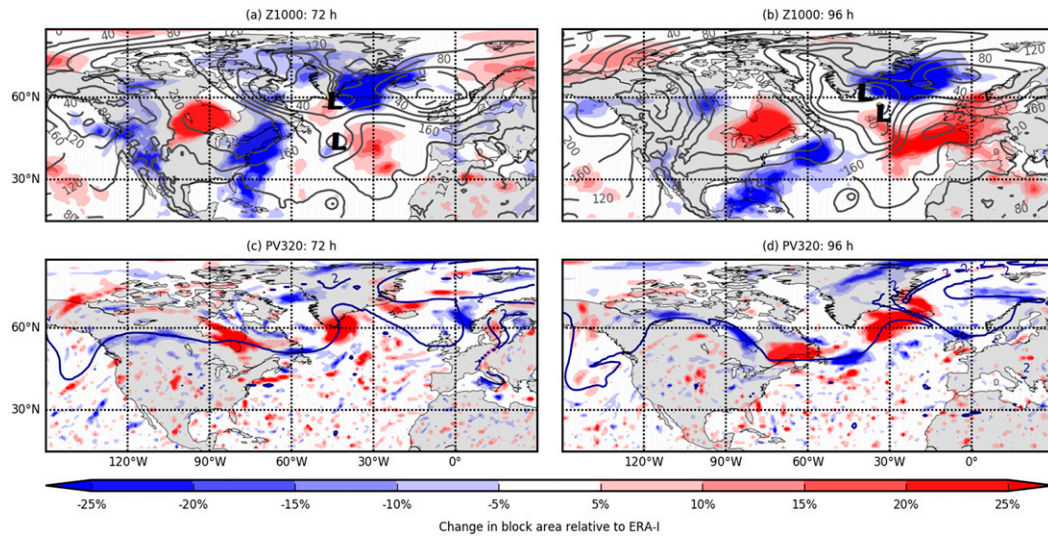
FIG. 6. Sensitivity of the response function 144 h into the forecast initiated at 1200 UTC 21 Sep 2015 to Z1000 at (a) 72- and (b) 96-h lead time and PV320 at (c) 72- and (d) 96-h lead time. The control member forecast of (a),(b) Z1000 or (c),(d) the 2-PVU contour is overlain.

this region than in the control member have a larger block form over the United Kingdom in the forecast. Larger PV320 in this region could be associated with a smaller ridge or an enhanced cyclonic overturning of the PV contour. By 96 h (Fig. 6d), the ridge–trough system over Canada has amplified and the sensitivity in the region has increased. The region of negative–positive sensitivity in the ridge–trough system suggests that a more amplified ridge–trough feature over Canada is associated with a larger block developing downstream over the United Kingdom.

In summary, ensemble sensitivity analysis indicates that the uncertainty in the ECMWF EPS for the NAWDEX dry run onset was associated with several upstream features. The area of the block forecast in the ensemble was sensitive to the following: Z1000 upstream over the Atlantic in the region of several low pressure systems, Z1000 over North America, PV320 along the western flank of the blocking ridge where WCB outflow from an upstream cyclone was located, and PV320 farther upstream in the region of another large-scale ridge–trough system.

5. Uncertain TIGGE block onsets

Ensemble sensitivities are now calculated for the 20 most uncertain block onsets over the Euro-Atlantic region during the study period (defined in section 2a). The most uncertain block onsets were defined as those that had the largest spread in the 6-day forecast of the area blocked in the ECMWF EPS on the date of block onset in the analysis (section 2). The two case studies

included in the previous sections are among this list of 20 uncertain block onset forecasts.

a. Hemispheric sensitivity

The sensitivity of the response function in each case to Z1000 two days prior to block onset is shown in Fig. 7. Note that in each case the blocked region corresponds to the upper-right corner of the figure (marked by the black box in Fig. 7a) and that the cases are grouped, as described, according to the location of the block: Greenland, the United Kingdom, or Scandinavia. The feeder cyclones that amplified the blocking ridges, identified using trajectory analysis, are indicated with an "L."

The patterns and magnitudes of sensitivity are different in each onset case. The magnitude of the sensitivity values is dependent on the area of the block in ERA-I because we present the results as a percentage change in this area to reflect the relative influence of the cyclone in each onset case. Presenting the sensitivity as an absolute value of block area change does not change the interpretation of the results included in this section. Although the patterns are different, common features exist: the region of highest sensitivity is located upstream of the block location, rather than over a large part of the Northern Hemisphere, and there is usually a cyclone (or cyclones) located upstream over the Atlantic Ocean. Three sensitivity patterns occur: (i) large-scale wave train–like patterns extending far upstream (Figs. 7g–k,m,n), (ii) more localized sensitivity just upstream of where the block forms (Figs. 7a–e, l,o,q–t), and (iii) little sensitivity across the whole domain (Figs. 7f,p). In several onset cases there is also increased
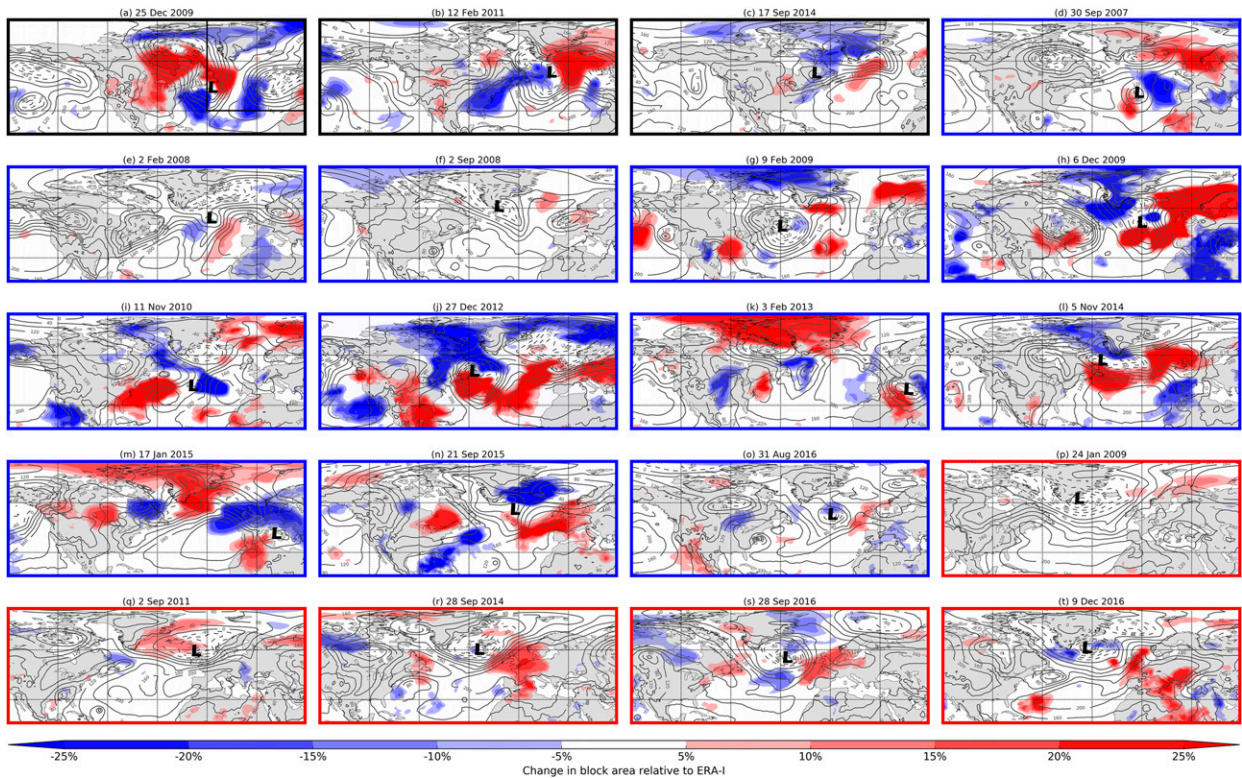
FIG. 7. Sensitivity of the block area in the ensemble at 144 h to Z1000 at 96 h for the 20 onset cases. Block onsets are separated into those occurring over Greenland (black map boundary), the United Kingdom (blue map boundary), and Scandinavia (red map boundary). The control member forecast of Z1000 is overlain in contours (every 40 m). The date shown for each onset date is the date that the forecast was initiated.

sensitivity to cyclone activity in the Mediterranean. Because the ensemble sensitivity analysis shows an association (rather than causality) between the representation of blocking and an earlier forecast of Z1000, it is no surprise that in some cases the sensitivity extends far upstream in a wavelike feature (Figs. 7g–k,m,n). For the Rossby wave structure (including the block) to be well represented over Europe, the large-scale trough–ridge structure will have to be in the correct location and phase as well. Block onsets over Europe are frequently supported by a quasi-stationary Rossby wave train coming from the subtropical western Atlantic (Nakamura et al. 1997). This pattern would be associated with surface activity (such as cyclones) in several upstream regions.

The sensitivity to PV320 two days prior to block onset in each case is shown in Fig. 8. Again, the pattern and magnitude of sensitivity is different in each case. The commonality between cases is that the sensitivity is focused generally along the 320-K tropopause, often in bands aligned with the tropopause, and that it generally has maximum magnitude around the ridge that becomes the block. The sensitivity to PV320 on either side of the tropopause indicates spread in the ensemble forecast in

this location has a large downstream effect. Spread in the ensemble in PV320 near the tropopause could develop from one or more of the five mechanisms of proposed near-tropopause PV error growth found in a case study by Davies and Didone (2013). We expect diabatic processes to modify the PV structure near the tropopause (e.g., Joos and Wernli 2012; Chagnon et al. 2013) so the increased sensitivity in each case near the tropopause could also imply that the diabatic processes within each ensemble representation of the cyclones are the cause of this sensitivity. Furthermore, this increased sensitivity to PV is often in the ridge ahead of the surface cyclone that was associated with large sensitivity, implying the sensitivities are highlighting real dynamical features that are important for block formation and not spurious sensitivities occurring as a consequence of our relatively small ensemble. The sensitivity of block onset to upstream cyclone representation in the ensemble can be inferred from both sensitivity fields. However, some onsets show little sensitivity to either field. This implies that the uncertainty in the ensemble forecast of these onsets of blocking at six days lead time was not associated with increased spread in the earlier forecast of Z1000 or PV320. This does not necessarily imply that the
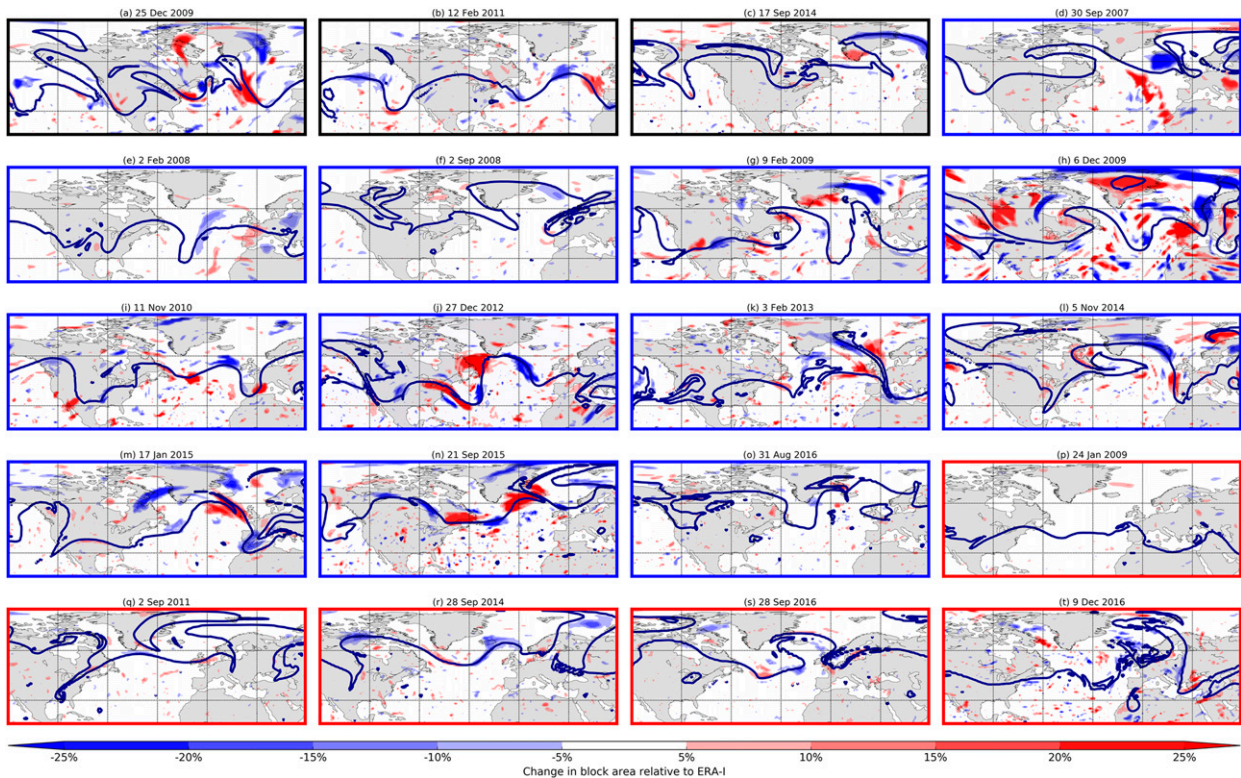
FIG. 8. As in Fig. 7, but for sensitivity to PV320. The control member forecast of the 2-PVU contour is overlain.

forecast was not sensitive to cyclone structure because Z1000 and PV320 cannot describe a cyclone's structure fully. Influence from the stratosphere or more local effects could also be important in these cases. There are also some onsets that show sensitivity to one field but not the other, for example, for the onset forecast from 2 September 2011 (Figs. 7q, 8q).

The aim of this part of the study was to determine the impact of the forecast of upstream cyclones on the downstream representation of blocking in uncertain medium-range forecasts. Even though in many of the block onset cases there is large sensitivity in the region upstream of the block around one or more cyclones, the sensitivity in the region of the feeder cyclone for the majority of the block onset cases is as large (or larger) than sensitivity in other regions. This indicates that cyclone

representation is of first-order importance for downstream block forecast.

b. Ensemble sensitivity for alternative function results

Sensitivity to Z1000 and PV320 for each onset case was also calculated for the RMSE of Z500 and ridge area response functions described in section 2c(2). The general features identified using the block area as the response function are present in both other response functions: the sensitivity field to Z1000 resembles either a large wave train pattern extending far upstream, a localized region of sensitivity near an upstream cyclone, or reduced sensitivity across the domain; and the sensitivity to PV320 is focused along the tropopause. Results of the ensemble sensitivity analysis are summarized in Table 1. The majority of block onset

TABLE 1. The sensitivity patterns using RMSE Z500 and ridge area as the response functions are compared to those using block area as the response function. The numbers indicate the number of cases (of the 20 studied) for which the sensitivity fields are similar (first and third columns of numbers) and the number of cases, for all three response functions, where there is locally increased sensitivity near to a specific feature (second and fourth columns).

Response function	Similar pattern in sensitivity to Z1000 as block area	Increased sensitivity near upstream cyclone	Similar pattern in sensitivity to PV320 as block area	Increased sensitivity to upper-level ridge
Block area	—	17	—	16
RMSE Z500	13	14	16	12
Ridge area	14	13	16	14

cases have similar patterns in sensitivity to those shown in Figs. 7 and 8 for both the RMSE of Z500 and ridge area response functions. Similarity between patterns is based on large-scale sensitivity patterns identified by eye. Large sensitivity near the upstream feeder cyclones and around the upper-level blocking ridges is also found for both additional response functions, though in fewer of the cases than with the block area response function. The consistency in sensitivity patterns between response functions used in the sensitivity analysis demonstrate that the result that the forecast of block onset is sensitive to the representation of upstream cyclones is robust to the definition of response function.

c. Feeder cyclone sensitivity

To analyze the sensitivity to each block's feeder cyclone in more detail, the sensitivity maps are now restricted to a $30° \times 30°$ domain centered on the cyclone at the lead time for which the sensitivity was greatest; this time is either two or three days prior to the analyzed block onset (i.e., at 72 or 96 h), and so differs from Fig. 7 for which 96 h is used for all panels. The ordering of panels is also changed and is grouped based on the type of sensitivity pattern found in the feeder cyclone restricted domains. In the cases where more than one cyclone was identified as ridge building, the cyclone with most trajectories ending in the block was selected. In most cases the feeder cyclones are located to the west of the block over the Atlantic. However, in the forecasts of block onset valid on the 3 February 2013 (Fig. 9e) and 17 January 2015 (Fig. 9g) it is a Mediterranean cyclone to the south of the block that contributed most to ridge building and was associated with the large sensitivity. Three characteristic patterns of sensitivity to the upstream cyclone emerge from Fig. 9. The block onsets have sensitivity to an upstream cyclone with any of the following:

(i) A dipole of sensitivity either side of the cyclone center (Figs. 9a–n). These can be oriented with positive sensitivity to the east of the cyclone and negative to the west or vice versa, as well as with positive sensitivity to the north and negative to the south and vice versa. There is no obvious dominant orientation.
(ii) A monopole of sensitivity in the location around the cyclone (Figs. 9o–q).
(iii) Little sensitivity in the location of the cyclone (Figs. 9r–t).

The block onsets that have a dipole in sensitivity around the feeder cyclone were influenced by the earlier forecast of the location and/or intensity of their feeder cyclone as can be inferred using the results of the idealized sensitivities [section 2c(3)] as follows. For the

onsets that have quasi-symmetric dipoles around the cyclone (e.g., Figs. 9f,i) it was the forecast location of the cyclone among the ensemble that was associated with the biggest change in block area forecast. Onsets with one lobe of the dipole larger or of greater magnitude were sensitive to both the location and the intensity of the cyclone in the forecast: if the positive lobe dominates it is the less intense systems that result in more blocking, and vice versa. If the dipole is oriented with negative sensitivity ahead of the cyclone it is the systems farther to the east that result in a large block; positive sensitivity ahead implies it is the cyclones farther west. When there is a monopole in sensitivity near the location of the feeder cyclone this implies the cyclone's intensity was most important for downstream block development sensitivity. Of the 20 block onset cases considered, 14 have a dipole in sensitivity (8 with positive–negative orientation, 6 with negative–positive), 3 onsets resemble monopoles, and 3 onsets have little sensitivity to the upstream feeder cyclone.

These patterns of sensitivity demonstrate that the location or intensity (or both) of an upstream cyclone two or three days prior to block onset is important in the forecast of blocks that showed largest uncertainty during recent years. Of the 20 onsets that had the largest spread in their 6-day forecast of block onset, 17 had large sensitivity to an upstream feeder cyclone: a one standard deviation change in Z1000 is associated with a 20%–25% change in block area. The results also show that upstream cyclones are not always important for unpredictable block onsets over the North Atlantic and Europe.

d. The relationship between cyclone characteristics and ensemble sensitivity

In this section we assess the relationship between characteristics of the feeder cyclones and total ensemble sensitivities in each of the 20 block onset cases. For each case we correlate spatially summed ensemble sensitivities for Z1000 and PV320 and also correlate these sensitivities with feeder cyclone characteristics. The sum over the domain of the magnitude of the sensitivity at each grid point (termed total sensitivity) is our sensitivity metric. For example, the total sensitivity to Z1000 at 96 h for the first case shown in Fig. 7 is calculated by summing the magnitude of the sensitivity values at each grid point in Fig. 7a. This simple metric provides a single value of total sensitivity (i.e., uncertainty in block area associated with Z1000 or PV320) for each of the onset cases at each lead time. We use magnitude of minimum Z1000 (in the control forecast) at 72 and 96 h as measures of cyclone intensity and number of WCB trajectories within the 72 h before block onset (in the
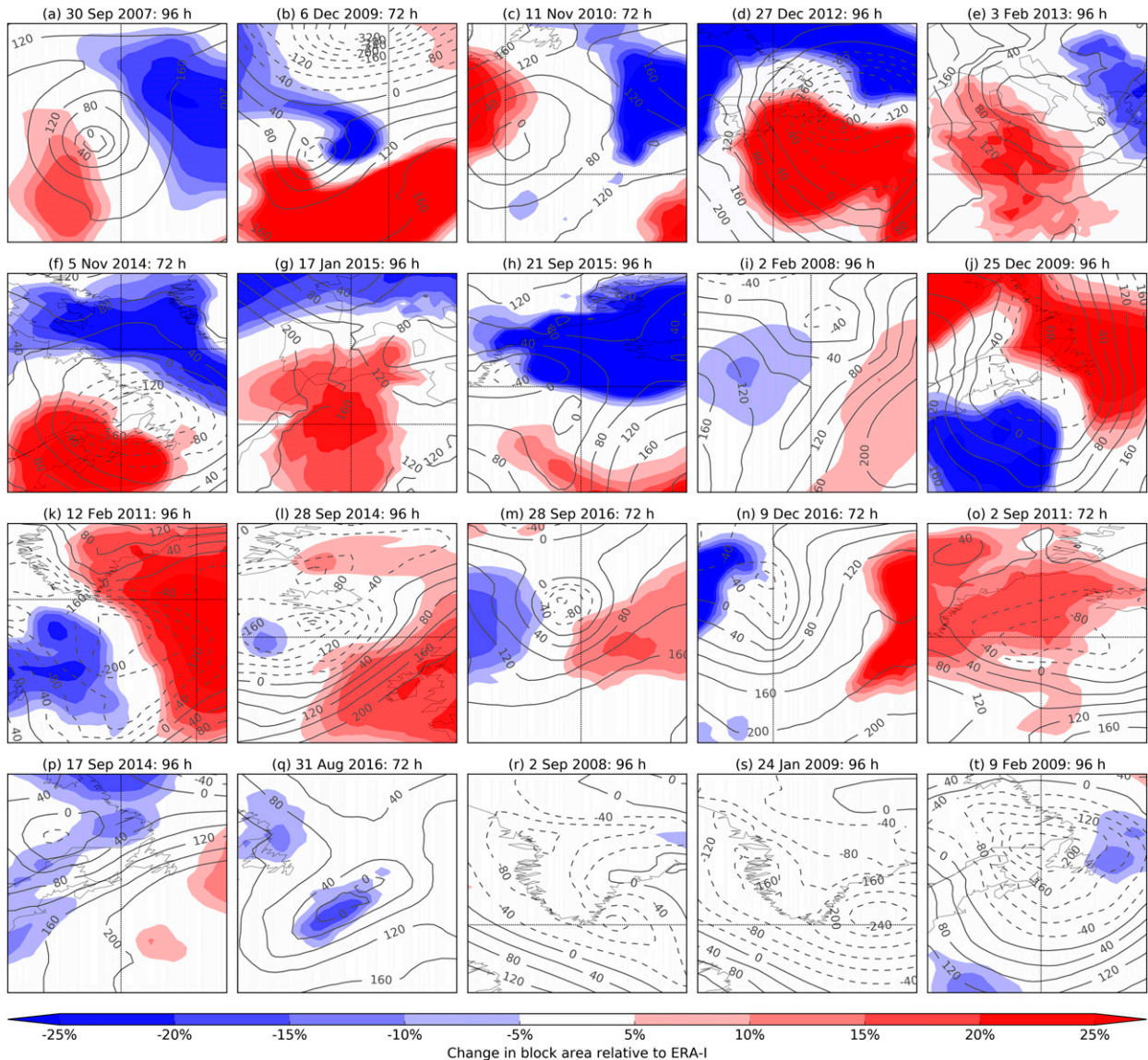
FIG. 9. Sensitivity of the block area at 144 h to Z1000 in the region of the upstream feeder cyclone at 72- or 96-h lead time (whichever time the sensitivity was greater). For the onsets that have maximum sensitivity at 96 h the data shown are a zoomed-in version of that shown in Fig. 7. The control forecast of Z1000 is overlain in contours.

ECMWF operational analysis) as a measure of WCB intensity. Total sensitivity to Z1000 and PV320 are highly correlated with themselves (significant at the 10% level) for different lead times as well as with each other at the same and different lead times. PV320 has higher correlation when comparing its sensitivity at 72 and 96 h (0.964) than Z1000 (0.834). When comparing the different fields, the correlation between sensitivity to Z1000 at 72 h and sensitivity to PV320 at 96 h is the highest (0.938), with the correlation between sensitivity to PV320 at 72 h to Z1000 at 96 h the lowest (0.792). This result supports the hypothesis that in the block onset

cases sensitivity to surface cyclones evolves with the flow to become sensitivity to the upper-level Rossby wave pattern (likely via changes to WCB representation).

Total sensitivity to either Z1000 or PV320 is not significantly correlated with cyclone intensity at either lead time. This implies that the degree of uncertainty in block size associated with feeder cyclone location and/or intensity, or upper-level Rossby wave pattern, does not depend on feeder cyclone intensity in our 20 cases. Total sensitivity to PV320 at 72 and 96 h are both significantly correlated to WCB intensity (0.438 and 0.384 respectively), whereas total sensitivity to Z1000 is not

significantly correlated with WCB intensity at either lead time. The significant correlations found between WCB intensity and total sensitivity to PV320 further support our hypothesis that the high sensitivity of block area to PV320 in the ensemble arises from the modification of the upper-level Rossby wave structure by WCBs.

6. Conclusions

The importance of cyclone representation in uncertain medium-range forecasts of block onset over the Euro-Atlantic region in the ECMWF EPS has been assessed systematically over many forecasts here for the first time using ensemble sensitivity analysis. The onset of blocking has been shown to be sensitive to upstream features previously in several different models and using a variety of methods (e.g., Yang et al. 1997; Frederiksen 1998; Frederiksen et al. 2004; Matsueda et al. 2011), though normally for single case study events. In this study we focus on the relationship between uncertainty in operational NWP model forecasts of blocking and upstream cyclones in a larger set of case studies. The effect surface cyclone representation can have on the downstream block forecast has been illustrated in two case studies of block onset over Europe related to the NAWDEX field campaign (Schäfler et al. 2018). Differing cyclone intensity and location among the ensemble in the days prior to block onset was associated with different Rossby wave evolution and block formation (or not). Ensemble sensitivity analysis was used to verify that the ensemble forecast of the block onsets was sensitive to changes in the upstream surface geopotential height pattern as well as to changes in PV in the region around the tropopause. The sensitivity to PV was generally strongest around the edge of ridges, which is where we expect diabatic outflow of WCBs to have a strong impact.

To investigate this case dependence in more detail, the relationship between block onset and upstream cyclone activity has been studied using ensemble sensitivity analysis for 20 cases (including the two cases described above) of block onset over the Euro-Atlantic region that had large ensemble spread in their 6-day forecasts. The forecasts of block onset were shown to be generally sensitive to the upstream surface geopotential height pattern and upper-level PV field in the days preceding the block onset. The sensitivity to Z1000 was largest upstream of the block location and typically associated with a surface cyclone, usually over the North Atlantic though in two cases over the Mediterranean. The sensitivity pattern sometimes extended far upstream implying, as to be expected, that the hemispheric

phasing of Rossby waves associated with surface weather upstream is important for block formation in a given region. The sensitivity to PV320 was generally greatest near the tropopause (2-PVU contour), where diabatic processes in extratropical cyclones modify the PV structure. Significant correlations were found between the total sensitivity to Z1000 and PV320 in the 20 cases. The total sensitivity to PV320 in the ensemble was shown to be positively correlated to the intensity of the WCB of the feeder cyclone in the ECMWF operational analysis. However, the total sensitivity to PV320 and Z1000 did not depend on the intensity of the feeder cyclone in the control forecasts.

To focus on the importance of upstream cyclone forecasts, the sensitivities were calculated in the region of each block onset's upstream feeder cyclone (established from the WCBs identified by back trajectories from within the block) at the time the block area exhibited maximum sensitivity to the cyclone. Blocks associated with more than one cyclone were prescribed a primary feeder cyclone based on the WCB that had the most trajectories. The forecast location and intensity of the upstream cyclone is shown to strongly influence block formation in 17 of the 20 onset cases considered. Changes in the ensemble forecast of geopotential height in the region of an upstream cyclone in the Atlantic were shown to be associated with a large change in the forecast block area: 20%–25% of the area of the block in ERA-I. The pattern of sensitivity is different for each case, suggesting that there is no systematic error in block onset related to upstream cyclone forecast. The relative importance of cyclone intensity and location for block formation was interpreted using sensitivity patterns generated using idealized cyclones: 14 of the 20 block onset cases had a dipole in sensitivity around their feeder cyclone implying that the forecast location dominated the impact on downstream block development with some importance of intensity of the cyclone for asymmetric dipoles, 3 of the cases had a monopole in sensitivity implying that the forecast of cyclone intensity was most important, and the remaining 3 cases had little sensitivity near the cyclone.

The results presented in this study are generally consistent with the large body of work investigating upstream influences on block dynamics. The demonstrated sensitivity to large-scale wave train–like features extending from the subtropics suggest that the importance of low-frequency Rossby wave trains in analyzed blocking events over Europe (Nakamura et al. 1997) is also important in the forecast of block onset over Europe. The sensitivity of block formation over the North Atlantic to upstream perturbations off the coast of North America, found when examining instabilities of

the flow in quasigeostrophic models (Frederiksen and Bell 1990; Frederiksen 1998), is consistent with the sensitivity in an operational EPS found here. Colucci (1987) and Lupo and Smith (1995) highlight the existence of an upstream cyclone in all their considered cases of analyzed blocking events: we find this is also true for the forecast of the 20 block onset cases included here. The conclusion that uncertain forecasts of block onset are sensitive to upstream cyclones is directly comparable with Magnusson (2017). The sensitivity of a blocking event (a forecast bust in ERA-I) to Z500 was highest upstream in the western Atlantic and was linked to the poor forecast of a cyclone developing in the same region. Here we have looked at the sensitivity of many block onset cases to Z1000 and demonstrated that cyclone representation is associated with large forecast sensitivity in the majority of cases. This result implies that cyclone representation could have a large influence on forecast busts over Europe and that better representation of the cyclones could help reduce the frequency of forecast busts that are associated with block onset. The results presented here are also consistent with Matsueda et al. (2011) who showed that a block over the Rockies was sensitive to an upstream cutoff cyclone in the Pacific.

Using ensemble sensitivity analysis we have shown that block onset forecasts are often limited by the forecast of an upstream surface cyclone. The question then arises of why the cyclone forecasts are uncertain. Sensitivity along the waveguide farther upstream of the cyclones in many cases suggests that transient upper-level features may also be associated with the increased uncertainty in the cyclone development and downstream influence. Diabatic processes are often intense in the WCBs of extratropical cyclones and have also been shown to affect cyclone development (e.g., Joos and Wernli 2012). For example, the low-level, diabatically produced positive PV anomaly beneath the region of maximum heating was shown to contribute about 40% to the circulation in a mature cyclone by Davis and Emanuel (1991). In NWP models diabatic processes need to be parameterized and different parameterizations have also been shown to result in different WCB development (Martínez-Alvarado and Plant 2014). The parameterization of diabatic processes in extratropical cyclones are a source of model uncertainty in addition to initial condition, boundary condition, and other model uncertainties. Future work should investigate the relationship between parameterized physical processes in NWP models and the downstream development of blocking and determine if different or better parameterizations can reduce the uncertainty in forecasts of block onset.

REFERENCES

Ahmadi-Givi, F., G. Graig, and R. Plant, 2004: The dynamics of a midlatitude cyclone with very strong latent-heat release. *Quart. J. Roy. Meteor. Soc.*, **130**, 295–323, https://doi.org/10.1256/qj.02.226.

Altenhoff, A. M., O. Martius, M. Croci-Masploi, C. Schwierz, and H. C. Davies, 2008: Linkage of atmospheric blocks and synoptic-scale Rossby waves: A climatological analysis. *Tellus*, **60A**, 1053–1063, https://doi.org/10.1111/j.1600-0870.2008.00354.x.

Ancell, B., and G. J. Hakim, 2007: Comparing adjoint-and ensemble-sensitivity analysis with applications to observation targeting. *Mon. Wea. Rev.*, **135**, 4117–4134, https://doi.org/10.1175/2007MWR1904.1.

Anstey, J. A., and Coauthors, 2013: Multi-model analysis of Northern Hemisphere winter blocking: Model biases and the role of resolution. *J. Geophys. Res. Atmos.*, **118**, 3956–3971, https://doi.org/10.1002/jgrd.50231.

Austin, J., 1980: The blocking of middle latitude westerly winds by planetary waves. *Quart. J. Roy. Meteor. Soc.*, **106**, 327–350, https://doi.org/10.1002/qj.49710644807.

Binder, H., M. Boettcher, H. Joos, and H. Wernli, 2016: The role of warm conveyor belts for the intensification of extratropical cyclones in Northern Hemisphere winter. *J. Atmos. Sci.*, **73**, 3997–4020, https://doi.org/10.1175/JAS-D-15-0302.1.

——, ——, C. M. Grams, H. Joos, S. Pfahl, and H. Wernli, 2017: Exceptional air mass transport and dynamical drivers of an extreme wintertime Arctic warm event. *Geophys. Res. Lett.*, **44**, 12 028–12 036, https://doi.org/10.1002/2017GL075841.

Bougeault, P., and Coauthors, 2010: The THORPEX Interactive Grand Global Ensemble. *Bull. Amer. Meteor. Soc.*, **91**, 1059–1072, https://doi.org/10.1175/2010BAMS2853.1.

Buizza, R., M. Milleer, and T. Palmer, 1999: Stochastic representation of model uncertainties in the ECMWF Ensemble Prediction System. *Quart. J. Roy. Meteor. Soc.*, **125**, 2887–2908, https://doi.org/10.1002/qj.49712556006.

Carrera, M., R. Higgins, and V. Kousky, 2004: Downstream weather impacts associated with atmospheric blocking over the northeast Pacific. *J. Climate*, **17**, 4823–4839, https://doi.org/10.1175/JCLI-3237.1.

Chagnon, J., S. Gray, and J. Methven, 2013: Diabatic processes modifying potential vorticity in a North Atlantic cyclone. *Quart. J. Roy. Meteor. Soc.*, **139**, 1270–1282, https://doi.org/10.1002/qj.2037.

Colucci, S. J., 1985: Explosive cyclogenesis and large-scale circulation changes: Implications for atmospheric blocking. *J. Atmos. Sci.*, **42**, 2701–2717, https://doi.org/10.1175/1520-0469(1985)042<2701:ECALSC>2.0.CO;2.

——, 1987: Comparative diagnosis of blocking versus nonblocking planetary-scale circulation changes during synoptic-scale cyclogenesis. *J. Atmos. Sci.*, **44**, 124–139, https://doi.org/10.1175/1520-0469(1987)044<0124:CDOBVN>2.0.CO;2.

——, and T. L. Alberta, 1996: Planetary-scale climatology of explosive cyclogenesis and blocking. *Mon. Wea. Rev.*, **124**, 2509–2520, https://doi.org/10.1175/1520-0493(1996)124<2509:PSCOEC>2.0.CO;2.

Dacre, H. F., and S. L. Gray, 2013: Quantifying the climatological relationship between extratropical cyclone intensity and atmospheric precursors. *Geophys. Res. Lett.*, **40**, 2322–2327, https://doi.org/10.1002/grl.50105.

Davies, H. C., and M. Didone, 2013: Diagnosis and dynamics of forecast error growth. *Mon. Wea. Rev.*, **141**, 2483–2501, https://doi.org/10.1175/MWR-D-12-00242.1.

Davini, P., and F. D'Andrea, 2016: Northern Hemisphere atmospheric blocking representation in global climate models: Twenty years of improvements? *J. Climate*, **29**, 8823–8840, https://doi.org/10.1175/JCLI-D-16-0242.1.

Davis, C. A., and K. A. Emanuel, 1991: Potential vorticity diagnostics of cyclogenesis. *Mon. Wea. Rev.*, **119**, 1929–1953, https://doi.org/10.1175/1520-0493(1991)119<1929:PVDOC>2.0.CO;2.

——, M. T. Stoelinga, and Y.-H. Kuo, 1993: The integrated effect of condensation in numerical simulations of extratropical cyclogenesis. *Mon. Wea. Rev.*, **121**, 2309–2330, https://doi.org/10.1175/1520-0493(1993)121<2309:TIEOCI>2.0.CO;2.

Dawson, A., and T. Palmer, 2015: Simulating weather regimes: Impact of model resolution and stochastic parameterization. *Climate Dyn.*, **44**, 2177–2193, https://doi.org/10.1007/s00382-014-2238-x.

Dee, D., and Coauthors, 2011: The ERA-Interim reanalysis: Configuration and performance of the data assimilation system. *Quart. J. Roy. Meteor. Soc.*, **137**, 553–597, https://doi.org/10.1002/qj.828.

Ferranti, L., S. Corti, and M. Janousek, 2015: Flow-dependent verification of the ECMWF ensemble over the Euro-Atlantic sector. *Quart. J. Roy. Meteor. Soc.*, **141**, 916–924, https://doi.org/10.1002/qj.2411.

Frederiksen, J. S., 1998: Precursors to blocking anomalies: The tangent linear and inverse problems. *J. Atmos. Sci.*, **55**, 2419–2436, https://doi.org/10.1175/1520-0469(1998)055<2419:PTBATT>2.0.CO;2.

——, and R. Bell, 1990: North Atlantic blocking during January 1979: Linear theory. *Quart. J. Roy. Meteor. Soc.*, **116**, 1289–1313, https://doi.org/10.1002/qj.49711649603.

——, M. A. Collier, and A. B. Watkins, 2004: Ensemble prediction of blocking regime transitions. *Tellus*, **56A**, 485–500, https://doi.org/10.1111/j.1600-0870.2004.00075.x.

Galarneau, T. J., Jr., T. M. Hamill, R. M. Dole, and J. Perlwitz, 2012: A multiscale analysis of the extreme weather events over western Russia and northern Pakistan during July 2010. *Mon. Wea. Rev.*, **140**, 1639–1664, https://doi.org/10.1175/MWR-D-11-00191.1.

Garcies, L., and V. Homar, 2009: Ensemble sensitivities of the real atmosphere: Application to Mediterranean intense cyclones. *Tellus*, **61A**, 394–406, https://doi.org/10.1111/j.1600-0870.2009.00392.x.

Grams, C. M., and H. M. Archambault, 2016: The key role of diabatic outflow in amplifying the midlatitude flow: A representative case study of weather systems surrounding western North Pacific extratropical transition. *Mon. Wea. Rev.*, **144**, 3847–3869, https://doi.org/10.1175/MWR-D-15-0419.1.

——, and Coauthors, 2011: The key role of diabatic processes in modifying the upper-tropospheric wave guide: A North

Atlantic case-study. *Quart. J. Roy. Meteor. Soc.*, **137**, 2174–2193, https://doi.org/10.1002/qj.891.

——, L. Magnusson, and E. Madonna, 2018: An atmospheric dynamics perspective on the amplification and propagation of forecast error in numerical weather prediction models: A case study. *Quart. J. Roy. Meteor. Soc.*, **144**, 2577–2591, https://doi.org/10.1002/qj.3353.

Gray, S. L., C. Dunning, J. Methven, G. Masato, and J. M. Chagnon, 2014: Systematic model forecast error in Rossby wave structure. *Geophys. Res. Lett.*, **41**, 2979–2987, https://doi.org/10.1002/2014GL059282.

Harvey, B. J., J. Methven, and M. H. Ambaum, 2016: Rossby wave propagation on potential vorticity fronts with finite width. *J. Fluid Mech.*, **794**, 775–797, https://doi.org/10.1017/jfm.2016.180.

Joos, H., and H. Wernli, 2012: Influence of microphysical processes on the potential vorticity development in a warm conveyor belt: A case-study with the limited-area model COSMO. *Quart. J. Roy. Meteor. Soc.*, **138**, 407–418, https://doi.org/10.1002/qj.934.

Jung, T., and Coauthors, 2010: The ECMWF model climate: Recent progress through improved physical parametrizations. *Quart. J. Roy. Meteor. Soc.*, **136**, 1145–1160, https://doi.org/10.1002/qj.634.

Kaas, E., and G. Branstator, 1993: The relationship between a zonal index and blocking activity. *J. Atmos. Sci.*, **50**, 3061–3077, https://doi.org/10.1175/1520-0469(1993)050<3061:TRBAZI>2.0.CO;2.

Kirsch, T. D., C. Wadhwani, L. Sauer, S. Doocy, and C. Catlett, 2012: Impact of the 2010 Pakistan floods on rural and urban populations at six months. *PLOS Curr.*, **1**, 2432, https://doi.org/10.1371/4fdfb212d2432.

Lillo, S. P., and D. B. Parsons, 2017: Investigating the dynamics of error growth in ECMWF medium-range forecast busts. *Quart. J. Roy. Meteor. Soc.*, **143**, 1211–1226, https://doi.org/10.1002/qj.2938.

Lupo, A. R., and P. J. Smith, 1995: Climatological features of blocking anticyclones in the Northern Hemisphere. *Tellus*, **47A**, 439–456, https://doi.org/10.3402/tellusa.v47i4.11527.

Madonna, E., H. Wernli, H. Joos, and O. Martius, 2014: Warm conveyor belts in the ERA-Interim dataset (1979–2010). Part I: Climatology and potential vorticity evolution. *J. Climate*, **27**, 3–26, https://doi.org/10.1175/JCLI-D-12-00720.1.

Magnusson, L., 2017: Diagnostic methods for understanding the origin of forecast errors. *Quart. J. Roy. Meteor. Soc.*, **143**, 2129–2142, https://doi.org/10.1002/qj.3072.

Martínez-Alvarado, O., and R. Plant, 2014: Parametrized diabatic processes in numerical simulations of an extratropical cyclone. *Quart. J. Roy. Meteor. Soc.*, **140**, 1742–1755, https://doi.org/10.1002/qj.2254.

——, E. Madonna, S. L. Gray, and H. Joos, 2016: A route to systematic error in forecasts of Rossby waves. *Quart. J. Roy. Meteor. Soc.*, **142**, 196–210, https://doi.org/10.1002/qj.2645.

——, J. W. Maddison, S. L. Gray, and K. D. Williams, 2018: Atmospheric blocking and upper-level Rossby wave forecast skill dependence on model configuration. *Quart. J. Roy. Meteor. Soc.*, **144**, 2165–2181, https://doi.org/10.1002/qj.3326.

Matsueda, M., 2009: Blocking predictability in operational medium-range ensemble forecasts. *SOLA*, **5**, 113–116, https://doi.org/10.2151/sola.2009-029.

——, R. Mizuta, and S. Kusunoki, 2009: Future change in wintertime atmospheric blocking simulated using a 20-km-mesh atmospheric global circulation model. *J. Geophys. Res.*, **114**, D12114, https://doi.org/10.1029/2009JD011919.

——, M. Kyouda, Z. Toth, H. Tanaka, and T. Tsuyuki, 2011: Predictability of an atmospheric blocking event that occurred on 15 December 2005. *Mon. Wea. Rev.*, **139**, 2455–2470, https://doi.org/10.1175/2010MWR3551.1.

Methven, J., 2015: Potential vorticity in warm conveyor belt outflow. *Quart. J. Roy. Meteor. Soc.*, **141**, 1065–1071, https://doi.org/10.1002/qj.2393.

Michel, C., and G. Rivière, 2011: The link between Rossby wave breakings and weather regime transitions. *J. Atmos. Sci.*, **68**, 1730–1748, https://doi.org/10.1175/2011JAS3635.1.

——, ——, L. Terray, and B. Joly, 2012: The dynamical link between surface cyclones, upper-tropospheric Rossby wave breaking and the life cycle of the Scandinavian blocking. *Geophys. Res. Lett.*, **39**, L10806, https://doi.org/10.1029/2012GL051682.

Molteni, F., R. Buizza, T. N. Palmer, and T. Petroliagis, 1996: The ECMWF Ensemble Prediction System: Methodology and validation. *Quart. J. Roy. Meteor. Soc.*, **122**, 73–119, https://doi.org/10.1002/qj.49712252905.

Mullen, S. L., 1987: Transient eddy forcing of blocking flows. *J. Atmos. Sci.*, **44**, 3–22, https://doi.org/10.1175/1520-0469(1987)044<0003:TEFOBF>2.0.CO;2.

Nakamura, H., and J. M. Wallace, 1993: Synoptic behavior of baroclinic eddies during the blocking onset. *Mon. Wea. Rev.*, **121**, 1892–1903, https://doi.org/10.1175/1520-0493(1993)121<1892:SBOBED>2.0.CO;2.

——, M. Nakamura, and J. L. Anderson, 1997: The role of high- and low-frequency dynamics in blocking formation. *Mon. Wea. Rev.*, **125**, 2074–2093, https://doi.org/10.1175/1520-0493(1997)125<2074:TROHAL>2.0.CO;2.

Palmer, T., G. Shutts, and R. Swinbank, 1986: Alleviation of a systematic westerly bias in general circulation and numerical weather prediction models through an orographic gravity wave drag parametrization. *Quart. J. Roy. Meteor. Soc.*, **112**, 1001–1039, https://doi.org/10.1002/qj.49711247406.

Pelly, J. L., and B. J. Hoskins, 2003: How well does the ECMWF Ensemble Prediction System predict blocking? *Quart. J. Roy. Meteor. Soc.*, **129**, 1683–1702, https://doi.org/10.1256/qj.01.173.

Pfahl, S., C. Schwierz, M. Croci-Maspoli, C. Grams, and H. Wernli, 2015: Importance of latent heat release in ascending air streams for atmospheric blocking. *Nat. Geosci.*, **8**, 610–614, https://doi.org/10.1038/ngeo2487.

Pithan, F., T. G. Shepherd, G. Zappa, and I. Sandu, 2016: Climate model biases in jet streams, blocking and storm tracks resulting from missing orographic drag. *Geophys. Res. Lett.*, **43**, 7231–7240, https://doi.org/10.1002/2016GL069551.

Rex, D. F., 1950: Blocking action in the middle troposphere and its effect upon regional climate. *Tellus*, **2**, 275–301, https://doi.org/10.3402/tellusa.v2i4.8603.

——, 1951: The effect of Atlantic blocking action upon European climate. *Tellus*, **3**, 100–112, https://doi.org/10.3402/tellusa.v3i2.8617.

Rodwell, M. J., and Coauthors, 2013: Characteristics of occasional poor medium-range weather forecasts for Europe. *Bull. Amer. Meteor. Soc.*, **94**, 1393–1405, https://doi.org/10.1175/BAMS-D-12-00099.1.

Scaife, A. A., T. Woollings, J. Knight, G. Martin, and T. Hinton, 2010: Atmospheric blocking and mean biases in climate models. *J. Climate*, **23**, 6143–6152, https://doi.org/10.1175/2010JCLI3728.1.

Schäfler, A., and Coauthors, 2018: The North Atlantic Waveguide and Downstream Impact Experiment. *Bull. Amer. Meteor. Soc.*, **99**, 1607–1637, https://doi.org/10.1175/BAMS-D-17-0003.1.

Scherrer, S. C., M. Croci-Maspoli, C. Schwierz, and C. Appenzeller, 2006: Two-dimensional indices of atmospheric blocking and their statistical relationship with winter climate patterns in the Euro-Atlantic region. *Int. J. Climatol.*, **26**, 233–250, https://doi.org/10.1002/joc.1250.

Schiemann, R., and Coauthors, 2017: The resolution sensitivity of Northern Hemisphere blocking in four 25-km atmospheric global circulation models. *J. Climate*, **30**, 337–358, https://doi.org/10.1175/JCLI-D-16-0100.1.

Shutts, G., 1983: The propagation of eddies in diffluent jet-streams: Eddy vorticity forcing of ''blocking'' flow fields. *Quart. J. Roy. Meteor. Soc.*, **109**, 737–761, https://doi.org/10.1002/qj.49710946204.

Sprenger, M., and H. Wernli, 2015: The LAGRANTO Lagrangian analysis tool—Version 2.0. *Geosci. Model Dev.*, **8**, 2569–2586, https://doi.org/10.5194/gmd-8-2569-2015.

Tamarin, T., and Y. Kaspi, 2016: The poleward motion of extratropical cyclones from a potential vorticity tendency analysis. *J. Atmos. Sci.*, **73**, 1687–1707, https://doi.org/10.1175/JAS-D-15-0168.1.

Tibaldi, S., and F. Molteni, 1990: On the operational predictability of blocking. *Tellus*, **42A**, 343–365, https://doi.org/10.3402/tellusa.v42i3.11882.

Torn, R. D., and G. J. Hakim, 2008: Ensemble-based sensitivity analysis. *Mon. Wea. Rev.*, **136**, 663–677, https://doi.org/10.1175/2007MWR2132.1.

Trigo, R., I. Trigo, C. DaCamara, and T. Osborn, 2004: Climate impact of the European winter blocking episodes from the NCEP/NCAR reanalyses. *Climate Dyn.*, **23**, 17–28, https://doi.org/10.1007/s00382-004-0410-4.

Tsou, C.-H., and P. J. Smith, 1990: The role of synoptic/planetary-scale interactions during the development of a blocking anticyclone. *Tellus*, **42A**, 174–193, https://doi.org/10.3402/tellusa.v42i1.11869.

Wernli, B. H., and H. C. Davies, 1997: A Lagrangian-based analysis of extratropical cyclones. I: The method and some applications. *Quart. J. Roy. Meteor. Soc.*, **123**, 467–489, https://doi.org/10.1002/qj.49712353811.

Woollings, T., and Coauthors, 2018: Blocking and its response to climate change. *Curr. Climate Change Rep.*, **4**, 287–300, https://doi.org/10.1007/s40641-018-0108-z.

Yamazaki, A., and H. Itoh, 2009: Selective absorption mechanism for the maintenance of blocking. *Geophys. Res. Lett.*, **36**, L05803, https://doi.org/10.1029/2008GL036770.

——, and ——, 2013: Vortex–vortex interactions for the maintenance of blocking. Part I: The selective absorption mechanism and a case study. *J. Atmos. Sci.*, **70**, 725–742, https://doi.org/10.1175/JAS-D-11-0295.1.

Yang, Y., Z. Li, and L. Ji, 1997: Adjoint sensitivity analyses on the anomalous circulation features in East Asian summer monsoon. *Adv. Atmos. Sci.*, **14**, 111–123, https://doi.org/10.1007/s00376-997-0050-9.

Zappa, G., G. Masato, L. Shaffrey, T. Woollings, and K. Hodges, 2014: Linking Northern Hemisphere blocking and storm track biases in the CMIP5 climate models. *Geophys. Res. Lett.*, **41**, 135–139, https://doi.org/10.1002/2013GL058480.